Reception Power Pattern of Distributed Absorbers in Focal Plane Arrays
A Fourier Optics Analysis

Llombart, Nuria; Dabironezare, Shahab Oddin; Carluccio, Giorgio; Freni, Angelo; Neto, Andrea

DOI
10.1109/TAP.2018.2862359

Publication date
2018

Document Version
Accepted author manuscript

Published in
IEEE Transactions on Antennas and Propagation

Reception Power Pattern of Distributed Absorbers in Focal Plane Arrays: a Fourier Optics Analysis

Nuria Llombart, *Senior Member*, *IEEE,* Shahab O. Dabironezare, *Student Member, IEEE*, Giorgio Carluccio, Angelo Freni, *Senior Member*, *IEEE* Andrea Neto, *Fellow, IEEE*

***Abstract*— Passive imaging cameras at millimeter and sub-millimeter wavelengths are currently entering a new era with the development of large format arrays of direct detectors. Several of these arrays are being developed with bare absorbing meshes without any antenna coupling (lens or horn) structures. The design of such arrays is typically done resorting to geometrical considerations or basic broadside plane wave incidence analysis. This paper presents a spectral technique for the analysis of such focal plane arrays in reception using Fourier Optics, which is valid also for moderately skewed incident angles. The analysis constitutes a step improvement with respect to previously used methods by providing an accurate and efficient way to estimate the point-source angular response and the throughput from a distributed incoherent source of an absorbing mesh in the focal plane of a quasi-optical component (e.g. a parabolic reflector or lens). The proposed technique is validated with full-wave simulations.**

After presenting the analysis, the paper compares the performance of arrays of bare absorber in the focal plane of a quasi-optical component to those of corresponding antenna based arrays. It is found that absorbers lead to a comparable trade-off, in terms of spill-over and focusing efficiency, only for very tight samplings. For larger samplings, the focusing efficiency of absorbers is significantly lower than the one for antennas.

Keywords—Submillimeter wave detectors, Quasi optics, Radiometry, Reflector antenna feeds.

I. Introduction

Sub-millimeter imagers for stand-off security applications are widely used to detect hazardous objects concealed under clothing [1]–[4]. Future security imagers will require larger Field of Views (FoVs), comparable to the size of a human body (i.e. images with over 100000 pixels), and video rate speeds (>10 Hz). The presence of many detectors in the focal plane of an optical system (e.g., charged coupled device (CCD) like configuration) enables the use of systems with none or very limited mechanical scanning. As a consequence, the requirement on the detector's sensitivity is relaxed, in such configuration, thanks to the possibility of using an integration time comparable to the frame rate. In the last years, there has been a significant effort in developing large format Focal Plane Arrays (FPAs) of bare absorbers based detectors with medium sensitivities for commercial sub-millimeter imaging cameras. Some current cameras make use of cryogenic Kinetic Inductance Detectors (KIDs) [5]–[9] or uncooled micro-bolometers [10], [11].

Traditionally, since the heat capacity of most bolometers scales with the area, antenna coupling structures have been used to reduce the bolometer physical dimension [12], at the cost of a more complex FPA architecture (e.g., fly's eye lens arrays [13] or horn arrays [14]). Instead, in [15], the use of FPAs of bare absorbers was proposed for tightly sampled large format configurations, i.e. in combination with optical systems with limited mechanical scanning. Such configurations have been recently implemented in astronomical instruments [7], and security imagers [8], [9]. There have been astronomical instruments developed with hybrid configurations such as multi-mode horns coupled to distributed absorbers [16], [17].

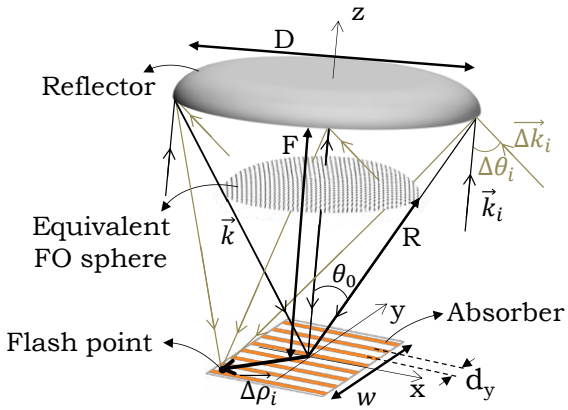

Fig. 1. The Fourier Optics scenario for broadside or oblique plane wave incidence onto a parabolic reflector with a square strip mesh absorber in its focal plane.

The trade-offs which dominate the design of focal plane arrays based on antenna feeds are well-known, [18], [19], especially when the systems are required to operate over narrow frequency bands. Focal plane arrays of bare absorbers are, however, much less studied. The amount of power received, and the obtainable angular resolution are significantly different from the one of antenna feeds. The difference raises from the fact that absorbers, unlike single port antennas, respond incoherently to multiple aperture field distributions induced by the incident field [20]. As a consequence, the effective area in absorbers cannot be related to the directivity as in the case of antennas. Section II discusses the effective area of an ideal absorber in comparison with that of antennas, highlighting that its value cannot be related to transmitting parameters such as directivity.

In [15], a basic study for deriving the trade-offs between the performances of bare absorbers and antennas was presented within the scope of astronomical instruments. In this

contribution, instead, an accurate analysis of FPAs based on bare absorbers is performed resorting to a spectral analysis technique that links the spectrum of the optical system to the one of the distributed absorber. The latter allows considering generic optical systems, even with low focal-to-diameter number, $f_{\#}$, (commonly referred also as F/D ratio [21]) and distributed absorbers. With respect to previous works, the terminology used here is more common to the reflector antenna community [19].

There have been several works [16], [17] that model distributed absorbers under multi-mode horns by combining mode matching techniques with a partially coherent summation of modes. Here, instead, we treated absorbers distributed directly in the focal plane. A schematic representation of the studied geometry is shown in Fig. 1. A canonical geometry of a symmetric parabolic reflector under plane wave illumination is chosen. Such geometry represents well the behavior of more complex multi-reflector systems for detectors closed to the focal point [21]. Moreover, the use of such geometry is commonly used to derive basic imaging system performance, and to compare different array elements [22], [23].

The tool used for the analysis of this canonical problem is described in Section III. It is based on a Fourier Optics (FO), [24], spectral field representation. The power received by a periodic absorber is evaluated by using a Floquet mode based equivalent circuit model similar to the one introduced in [25], whose generators are obtained by expanding the direct fields in terms of plane waves coming from the quasi-optical system (reflector in Fig. 1). In particular, the methodology in [25] is extended to skew incidence, and to any type of periodic absorber. The analysis of reflector systems in reception has also been used for characterizing antenna feeds [26], [27]. Using this approach, we accurately derive both the point source angular response of a bare absorber under a reflector, and the power received from an angularly distributed incoherent source.

In Section IV, the analysis of the power received from a point source as a function of the incident angle onto the optical system allows the introduction of *aperture* and *focusing efficiencies* of an absorber under an optical system. The aperture efficiency quantifies how much power is received from a broadside plane wave. The focusing efficiency quantifies how much the achieved angular response of the optical system is diffraction limited. It is worth noting that both of these efficiencies are calculated in reception.

For point sources, it turns out that the use of absorbers leads to a power received comparable to that obtained by antenna feeds, but at the cost of much lower focusing efficiency. The maximum of the product between the spill-over and focusing efficiency is 37% for absorbers with a dimension of $w = 1.2\lambda f_{\#}$, whereas in case of Gaussian antennas the maximum is 82% [28] for an antenna aperture dimension of about $2\lambda f_{\#}$. Therefore, an array of absorbers guarantees an effective use of the reflector area, comparable to that of antenna arrays, only in a highly populated FPAs with spacing $d \leq 0.75\lambda f_{\#}$.

In Section V, we derive the throughput, $A\Omega$, from an incoherent distributed source associated with an absorber located in the focal plane of an optical system. This term is typically adopted in optical research communities, and $A\Omega/\lambda^2$ is commonly referred to as the number of effective spatial modes, [20]. Here, the throughput is expressed in terms of antenna efficiencies. Whereas for single-mode antennas the throughput is bounded to $A\Omega \leq \lambda^2$, for absorbers it has an upper limit related to the reflector physical area (i.e. $A\Omega \leq \pi A_{ref}$) leading to a larger received power (or better sensitivity) with respect to antenna based FPAs, but at the cost of a reduced angular resolution.

In the literature, the term $A\Omega/\lambda^2$ is approximated resorting to basic radiometry calculations via geometrical approximations [29] or Airy pattern considerations [15]. Here, instead, a more rigorous methodology that makes use of an accurate evaluation of the angular response of the optical system is proposed. It includes coherence effects coming from the optics, such as phase errors due to the curvature of the optics, specially for low F/D ratios, or non-ideal absorber geometries, or changes in the frequency response because of resonant geometries, [8], [30].

The proposed method is validated in Section VI by full wave simulations. Section VII contains some concluding remarks. Finally, Appendix describes the model for the coupling of the absorbers to the optical system.

II. Effective Area in Absorbers

The powers received by antennas or absorbers due to an incident plane wave, P_r, can be evaluated via an effective area:

$$A_{eff}(\theta,\phi) = \frac{P_r(\theta,\phi)}{S_i}, \tag{1}$$

where $S_i = |E_0|^2/(2\zeta_0)$ is the incident power density, with ζ_0 being the free space wave impedance (377 Ω).

Antennas are typically characterized also by directivity transmitting patterns, and the corresponding effective area can be related to the directivity by $A_{eff}^{ant} = D_{ir}\lambda^2/4\pi$. Instead, the directivity is not a useful parameter to derive the effective area for electrically large distributed absorbers, since their radiation patterns cannot be related to a coherent aperture distribution. For this reason, it is more convenient to use the effective area as reference parameter for comparing the properties between antennas and absorbers.

An ideal electrically large planar absorber, see the inset of Fig. 3, can be achieved using a thin continuous sheet with a conductive material, σ, and thickness, h on top of quarter wavelength backshort, $h_{bs} = \lambda/4$ [31], [11]. The surface resistance of this sheet, since its thickness is smaller than the skin depth, can then be chosen to be $R_s = \zeta_0 = 1/(h\sigma)$ (Ω/□) [32].

To evaluate the power absorbed by such ideal absorber, one can use the equivalent circuit shown in Fig A.1, where the TE/TM equivalent lines are decoupled. For a generic plane wave incidence, $\vec{e}_i = E_0\hat{p}_i e^{-j\vec{k}_i\cdot\vec{r}}$, assuming that the back-short has no losses, and considering an electrically large absorber of area A, the power absorbed is the active power density flowing across any $z > 0$ transmission line cross section multiplied by the physical area of the absorber. After some algebraic manipulations, the absorbed power can be expressed as a function of the back short distance, h_{bs}, for each plane wave angle of incidence (θ_i, ϕ_i) and polarization $\hat{p}_i$, as follows:

$$P_{abs}^{PW}(\theta_i,\phi_i) = S_i A\cos\theta_i\left[\left(\hat{p}_i\cdot\hat{k}_{\rho i}\right)^2\chi_{TM} + \left(\hat{p}_i\cdot\hat{\phi}_i\right)^2\chi_{TE}\right] \quad (2)$$

where $\hat{k}_{\rho i} = \sin\theta_i\,(\cos\phi_i\,\hat{x} + \sin\phi_i\,\hat{y})$ and $\hat{\phi}_i = -\sin\phi_i\,\hat{x} + \cos\phi_i\,\hat{y}$. The efficiencies $\chi_{TM} = \frac{4\cos\theta_i}{(1+\cos\theta_i)^2+\cot^2(k_0\cos\theta_i h_{bs})}$ and $\chi_{TE} = \frac{4\cos\theta_i}{(1+\cos\theta_i)^2+\cos^2\theta_i\cot^2(k_0\cos\theta_i h_{bs})}$ take into account for the impact of the back short.

Figure 2 shows the normalized received power of the ideal planar absorber versus the plane wave angle of incidence for a standard back short distance, i.e. $\lambda/4$. Both a $\hat{\theta}$- and $\hat{\phi}$-polarized incident plane waves are considered. The curves differ from the standard *Lambert's cosine law*, commonly used in optics, due to the presence of the back short. The larger is the back short (e.g. as the ones used in [9]) the larger is the angular variation.

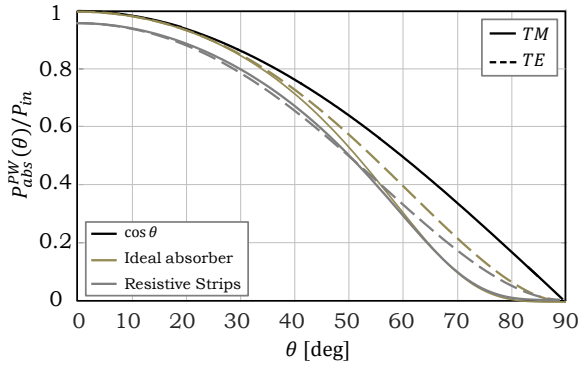

Fig. 2. Power absorbed by an ideal planar absorber and a strip absorber for a $\hat{\theta}$-(TM) and $\hat{\phi}$-polarized (TE) plane wave incidence at different incidence angles. Both designs use back shorts at $\lambda/4$ distance. The curves are normalized to $P_{in} = S_i A$.

Equation (2) shows that, for broadside plane wave incidence and $h_{bs} = \lambda/4$, the power received by the ideal absorber is the incident power density times the absorber area. Hence, for this case, the effective area is identical to the physical one. Instead for single mode[1] antennas the effective area can be related to the directivity by the relation $A_{eff}^{ant} = D_{ir}\lambda^2/(4\pi)$, where the directivity depends on the angular distribution of the antenna radiation pattern. Therefore, an antenna with an angular receiving power pattern of $\cos\theta$, similar to the one shown in Fig. 2, has an effective area of $A_{eff}^{ant} = \lambda^2/\pi$ irrespectively of its dimensions. In case of electrically large absorbers, the effective area, instead, increases linearly with the physical area, while having the same angular receiving pattern.

Figure 3 shows the effective area of the ideal absorber (with an infinite and a finite back short of the same size than the absorber). This effective area is reported as a function of the absorber's physical area calculated using full wave simulations done with CST MS [33] under broadside plane wave illumination. The simulated geometry is shown in the inset of the figure.

[1] Single mode antenna referred to antennas with a feeding port that excites a specific equivalent current distribution.

It is apparent that the effective area of absorbers matched to the wave impedance, ζ_0, remains equal to the physical area, even when the dimension of the overall absorber is small in terms of the wavelength. For the sake of comparison, the effective area of a matched antenna radiating above an infinite ground plane characterized by an equivalent electric current distribution $\vec{J}_a = rect(x,w/2)rect(y,w/2)\hat{x}$, is also shown in the same figure. For small dimensions, in terms of the wavelength, the antenna effective area can be much larger than the physical area. However, their designs are much more complex since they require the design of an impedance matching network which is frequency and dimension dependent.

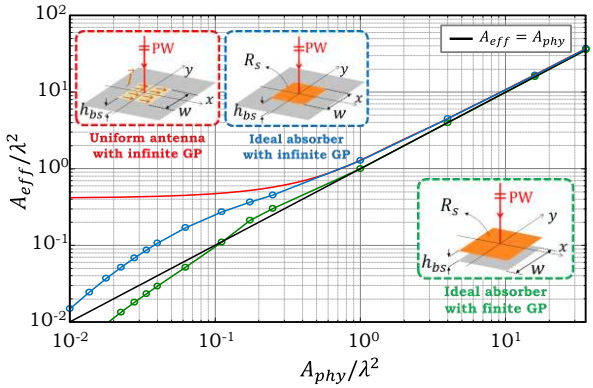

Fig. 3. Effective area of the ideal absorber (with an infinite and a finite back short of the same size than the absorber) versus the physical area compared to the effective area of an impedance matched antenna with uniform square electric distribution above an infinite ground plane. The distance to the back-short is $\lambda/4$ for all cases.

III. Fourier Optics Based Analysis

In [25] an analytical method, based on a Fourier Optics (FO) approach, for calculating the power absorbed by a resistive linear strip mesh in the focal plane of an optical system, was presented. The FO method can be used to derive in a simple way a spectral wave expansion of the direct field focused on the focal plane. For certain canonical optical configurations (e.g., parabolic reflector), an analytical expression of the spectrum can be derived. Other proposed approaches for deriving the spectrum resort to asymptotic procedures which make use of numerical evaluations of the Physical Optics (PO) field as in [34]. In [25], the spectral plane wave expansion derived by using FO was linked to a *periodic* spectral field representation in the surrounding of the absorbers (via a Floquet mode expansion [35]). In this section, the extension of the analysis to generic planar periodic absorbing geometries, and slightly off-broadside incidence, is presented. The mathematical derivation is shown in the Appendix, while in the following sections the extension will be used for the accurate estimation of both the aperture efficiencies, and the point-source responses of an imaging system based on bare absorber's FPAs.

Direct Field for Slightly Oblique Illumination

When an optical system is illuminated by a plane wave of amplitude, E_0, wave-vector $\overrightarrow{\Delta k}_i = k_0 \sin\Delta\theta_i\,(\cos\Delta\phi_i\,\hat{x} + \sin\Delta\phi_i\,\hat{y}) + k_0\cos\Delta\theta_i\,\hat{z}$ (Fig. 1), and polarization unit vector $\hat{p}_i$ (i.e., $\vec{e}_i(\vec{r}) = E_0\hat{p}_i e^{-j\overrightarrow{\Delta k}_i\cdot\vec{r}}$), an equivalent sphere centered at the focus of the focal plane can be used to evaluate a plane wave spectrum (PWS) representation of the *direct* focal field, $\vec{e}_d(\vec{\rho})$:

$$\vec{e}^{\,d}(\vec{\rho}) = \frac{1}{4\pi^2}\iint_{-\infty}^{+\infty}\vec{E}^{\,d}(\vec{k}_\rho)e^{j\vec{k}_\rho\cdot\vec{\rho}}\,k_\rho dk_\rho d\alpha \qquad (3)$$

where $\vec{E}^{\,d}(\vec{k}_\rho) = j2\pi R e^{-jkR}\vec{E}^{GO}(\vec{k}_\rho)/\sqrt{k^2-k_\rho^2}$, with R being the radius of the equivalent sphere (Fig. 1), $\vec{k}_\rho$ the spectral vector given by $\vec{k}_\rho = k_x\hat{x} + k_y\hat{y} = k_0\sin\theta\,(\cos\phi\,\hat{x} + \sin\phi\,\hat{y})$, and $\vec{E}^{GO}(\vec{k}_\rho)$ is the Geometrical Optics (GO) field [36] component tangent to the equivalent sphere. This GO field is only defined over the angular sector subtended by the optical system ($\theta \le \theta_0$), as shown in Fig. 1.

An analytical approximation of this field, and its limits of applicability, are given in [25] for a parabolic reflector with a focal distance, F, under broadside plane wave illumination, $\vec{e}_i = E_0\hat{p}_i e^{-jk_0 z}$. This approximation is taken here as the reference for the analysis. The field expression for a general polarization of a broadside incident plane wave is

$$\vec{E}^{GO}(\vec{k}_\rho, \overrightarrow{\Delta k}_{\rho i} = 0) = \frac{-2k_0E_0}{k_0+k_z}e^{-j\Delta k_{zi}F}\left[\hat{\theta}(\hat{p}_i\cdot\hat{k}_\rho) + \hat{\phi}(\hat{p}_i\cdot\hat{\alpha})\right]\mathrm{circ}(k_\rho, k_{\rho 0}) \qquad (4)$$

where $\hat{\alpha} = (-k_y\hat{x} + k_x\hat{y})/k_\rho$, $\Delta k_{\rho i}$ and Δk_{zi} are the ρ- and z-components of the incident wave vector, respectively; $k_{\rho 0} = k_0\sin\theta_0$, with θ_0 being the reflector subtended angle, and $\mathrm{circ}(k_\rho, k_{\rho 0})$ equals 1 for $|k_\rho| \le k_{\rho 0}$ and 0 elsewhere.

When an external plane wave is incident from a direction slightly off broadside, $(\Delta\theta_i, \Delta\phi_i)$, a key simplifying hypothesis, invoked typically in FO to evaluate the PWS in a computational efficient way, is that the polarization of the incident field $\vec{e}_i$, in the phase reference plane of the focusing system (Fig. 4), is the same as for the broadside plane wave case, while the progressive phase shift is explicitly accounted for. This means that the following expression of the incident plane wave applies along the phase reference plane:

$$\vec{e}_i(\overrightarrow{\Delta k}_{\rho i}) \simeq E_0 e^{-j\overrightarrow{\Delta k}_{\rho i}\cdot\vec{\rho}_i(\vec{r})}\hat{p}_i \qquad (5)$$

where $\overrightarrow{\Delta k}_{\rho i} = \Delta k_{xi}\hat{x} + \Delta k_{yi}\hat{y} = k_0\sin\Delta\theta_i\,(\cos\Delta\phi_i\,\hat{x} + \sin\Delta\phi_i\,\hat{y})$ is the transversal projection of the incident wave vector, $\overrightarrow{\Delta k}_i$, and $\vec{\rho}_i(\vec{r})$ represents the observation point in the phase reference plane (see Fig.4).

As discussed in [25], the field distribution on the equivalent sphere can be obtained by propagating the incident field via Geometrical Optics (GO) up to the equivalent sphere. Applying the approximation in (5), the GO field will be the same as broadside, except for a phase term:

$$\vec{E}^{GO}(\vec{k}_\rho, \overrightarrow{\Delta k}_{\rho i}) \simeq \vec{E}^{GO}(\vec{k}_\rho, \overrightarrow{\Delta k}_{\rho i} = 0)e^{-j\overrightarrow{\Delta k}_{\rho i}\cdot\vec{\rho}_i(\vec{r})} \qquad (6)$$

The approximation in (6) corresponds, for the worst polarization case, to neglect a field contribution proportional to $\tan\Delta\theta_i$. Retaining a 20% error on the field as tolerable, i.e. $\tan\Delta\theta_i < 0.2$, corresponds to an angular limitation $\Delta\theta_i < 11°$. The choice of 20% error in the GO field amplitude is consistent with the one taken in [25] for deriving the limits of the FO. This error choice assures that the field computed with the expressions given here matches the PO one with less than a 0.5 dB difference over the whole FO region of validity defined in [25].

As shown in the inset of Fig. 4, $\vec{\rho}_i = \rho_i\hat{k}_\rho$ can be parametrized with respect to an observation point on the FO equivalent sphere, $\vec{r} = R\hat{r}$, as

$$\vec{\rho}_i = \big(R + \delta_i(\theta)\big)\sin\theta\,\hat{k}_\rho \qquad (7)$$

where $\delta_i(\theta)$ quantifies the phase delay from the reflector surface to the equivalent sphere (see inset of Fig. 4) and we made use of the fact that $\hat{k}_\rho = \frac{\vec{k}_\rho}{k_0\sin\theta} = \hat{\rho}$. For a parabolic reflector this phase delay is $\delta_i(\theta) = 2F/(1+\cos\theta) - R$.

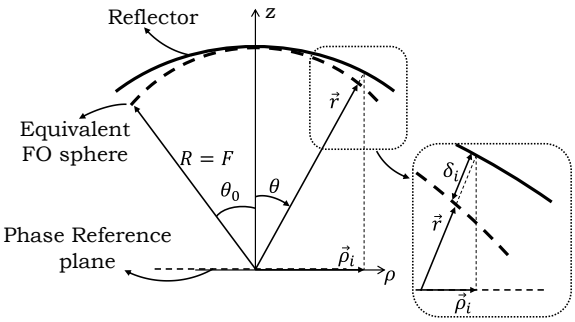

Fig. 4. Geometry to evaluate the phase term of the PWS for slightly off-broadside incidence with respect to a phase reference plane.

By substituting (7) into (6) we can observe two phase terms. The first phase term ($R\sin\theta\ \overrightarrow{\Delta k}_{\rho i}\cdot\hat{k}_\rho$) corresponds to a linear phase shift (beam steering) while the second one ($\delta_i\sin\theta\ \overrightarrow{\Delta k}_{\rho i}\cdot\hat{k}_\rho$) is a coma phase error (associated with asymmetric high side lobes [37]) coming from the curvature of the reflector. Assuming an equivalent sphere with the radius equal to the focal distance, i.e. $R = F$, the beam steering observed at the focal plane (here defined as the flash point, Fig. 1), $\overrightarrow{\Delta\rho}_i$, can be evaluated directly from the linear phase term as

$$\overrightarrow{\Delta\rho}_i = F\overrightarrow{\Delta k}_{\rho i}/k_0. \qquad (8)$$

The flash point in (8) quantifies the location of the peak of the field focalized in the focal plane by the optical system when the linear phase term is dominant. In Fig. 5 an example of the variation of the two phase terms is shown versus the spectral angle θ, when the plane wave incident on the reflector impinges

with a skewed angle with respect to broadside.

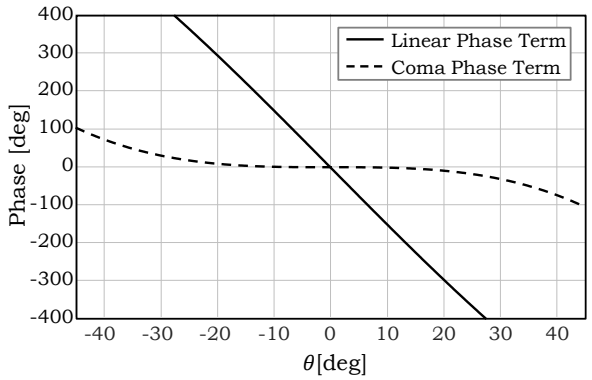

Fig. 5. Phase terms of the slightly off broadside PWS in case of a reflector with $f_{\#} = 0.6$ and $D = 100\lambda$ illuminated by a plane wave with $\Delta\theta_i/(\lambda/D) = 4$, $\Delta\phi_i = 0°$.

By using the approximation in (6), the phase term in the GO field can be expressed as a function of the spectral vector, $\vec{k}_\rho$, as follows:

$$e^{-j\overrightarrow{\Delta k}_{\rho i}\cdot\hat{\rho}\left(R+\delta_i(\theta)\right)\sin\theta} = e^{-j\overrightarrow{\Delta\rho}_i\cdot\vec{k}_\rho\left(1+\delta_n(\theta)\right)} \quad (9)$$

where $\delta_n(\theta) = \delta_i(\theta)/R = (1-\cos\theta)/(1+\cos\theta)$. In [38], it is shown that the dominant phase aberration in dual reflector systems is the coma one. This coma phase term is explicitly given in [39] for a paraboloid illuminated by an antenna feed. Typically, the coma phase term is given for the small angle approximation as cubic dependence of θ [40]. Therefore, the GO field in (4) can be expressed as function of the flash point position, as follows:

$$\vec{E}^{GO}\left(\vec{k}_\rho,\overrightarrow{\Delta k}_{\rho i}\right) \simeq \vec{E}^{GO}\left(\vec{k}_\rho,\overrightarrow{\Delta k}_{\rho i}=0\right)e^{-j\overrightarrow{\Delta\rho}_i\cdot\vec{k}_\rho\left(1+\delta_n(\theta)\right)} \quad (10)$$

The coma phase term, $\overrightarrow{\Delta\rho}_i\cdot\vec{k}_\rho\delta_n(\theta)$, in (10) can be neglected depending on the $f_{\#}$, and the numbers of scanned beams (i.e. $N = \Delta\theta_i/(\lambda/D)$). By imposing such coma phase term over the FO sphere to be smaller than $\pi/8$, we can evaluate the maximum number of scanned beams where the focalized field is almost a linear translation of the broadside one, i.e.:

$$N_{max}^{coma} = 0.25\left[f_{\#} + \sqrt{f_{\#}^2 - 0.25}\,\right]^2 \quad (11)$$

In Fig. 6 the field focalized in the focal plane by a parabolic reflector with $f_{\#} = 0.6$ is shown for two plane wave incidences: broadside and $\Delta\theta_i = 4\lambda/D$ (corresponding to 4 beams scanning). The field is evaluated with and without the coma phase term in the PWS, and compared with the field solution obtained by GRASP [41] when the PO solver option is used. It can be noted that the coma phase term changes the amplitude level of the first side lobe, and the location of the maximum field (not anymore given by (8)). It is evident that, for this low $f_{\#}$, the coma phase term cannot be neglected even for a single scanned beam, i.e. $N_{max}^{coma} \leq 1$, as derived in (11).

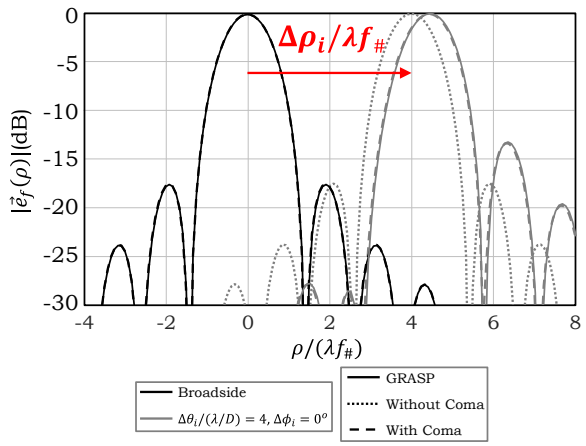

Fig. 6. Direct fields focalized by a reflector with $f_{\#} = 0.6$ and $D = 100\lambda$. The reflector is illuminated by two plane waves: at broadside and with $\Delta\theta_i/(\lambda/D) = 4$, $\Delta\phi_i = 0°$. Dash and dotted lines represent the fields with and without including the coma phase term in the PWS, respectively. The solid lines are relevant to the fields calculated with GRASP.

Evaluation of the Total Field

Following a procedure similar to the one highlighted in [25], and summarized in the Appendix, the coupling mechanism between the impinging field and the absorber can be represented via an equivalent Floquet circuit, see Fig. A1. The periodic absorbing mesh response to a plane wave is included in the circuit via an equivalent admittance matrix, $\bar{Y}_{abs}\left(\vec{k}_\rho\right)$. The components of this matrix can be derived analytically for a few structures as in [42] and [43], or evaluated numerically using periodic boundary conditions via a commercial electromagnetic tool such as CST MS, as in [44] and [35]. The input voltage waves, $V_+^{TE/TM}\left(\vec{k}_\rho\right)$, in the equivalent Floquet circuit can be related to the spectrum of the direct field coming from the optics, (3), by using (A.1) and (A.2). This methodology can be applied to any periodic structure embedded into a generic dielectric stratification (transverse to z-direction).

By solving the equivalent circuit, one can evaluate the spectral total average fields, $[\vec{E}^t, \vec{H}^t]$, at any z-quote, that includes both the absorber and optical system spectral responses. The spectral electric field, averaged over each absorber period (d_x, d_y), are related to the voltage solution, $V^{TE/TM}(\vec{k}_\rho, z)$, whereas the magnetic field to the current solution, $I^{TE/TM}(\vec{k}_\rho, z)$, as given in (A.5)–(A.8).

The spatial fields representing the response of the absorber to the optical system under a slightly off broadside incidence, $\vec{e}^t\left(\vec{\rho},\overrightarrow{\Delta k}_{\rho i}\right)$, can therefore be evaluated as the inverse Fourier transform of the spectral total field evaluated at broadside times the linear and coma phase terms:

$$\vec{e}^t\left(\vec{\rho},z,\overrightarrow{\Delta k}_{\rho i}\right) = \quad (12)$$
$$\frac{1}{4\pi^2}\iint_{-\infty}^{+\infty}\vec{E}^t\left(\vec{k}_\rho,z,\overrightarrow{\Delta k}_{\rho i}=0\right)e^{-j\vec{k}_\rho\cdot\overrightarrow{\Delta\rho}_i(1+\delta_n)}e^{j\vec{k}_\rho\cdot\vec{\rho}}k_\rho dk_\rho d\alpha$$

Only for the scanning angles imposed by (11), one can neglect the coma phase term, $\vec{k}_\rho\cdot\overrightarrow{\Delta\rho}_i\delta_n$, and the spatial fields

can be computed as a linear translation to the flash point, $\overrightarrow{\Delta\rho_i}$, of the broadside spatial total field:

$$\vec{e}^t\left(\vec{\rho}, z, \overrightarrow{\Delta k_{\rho i}}\right) \simeq \vec{e}^t(\vec{\rho} - \overrightarrow{\Delta\rho_i}, z, \overrightarrow{\Delta k_{\rho i}} = 0). \quad (13)$$

IV. Point-Source Response

In this section, we derive the response of resistive periodic absorber under a focusing system when the latter is illuminated by a single plane wave of amplitude E_0, impinging from a direction $\overrightarrow{\Delta k_i}$ (Fig. 1). Using (12), i.e. a coherent summation of the spectral total fields, averaged over each unit cell of the periodic absorber, we can estimate the total spatial electric and magnetic field, $\vec{e}^t(\vec{\rho}\,)$ and $\vec{h}^t(\vec{\rho}\,)$, at the focal plane. These fields are in effect evaluated as an inverse Fourier Transform of the PWS of the optical system times the spectral plane wave response of the absorber. The shape of the total fields depends on the response of the absorber to plane waves with incidence angles impinging from broadside up to the reflector subtended angle, θ_0. Once the fields are known, the power absorbed by a finite periodic mesh can be evaluated, assuming local periodicity, as the integral, over the absorber area w, of the z-component of the Poynting's vector associated with the spatial total fields, as follows:

$$P_{abs}\left(f, \overrightarrow{\Delta k_{\rho i}}\right) = \frac{1}{2} Re\left\{\iint_{-w/2}^{w/2} \left[\vec{e}_t\left(\vec{\rho}\,, \overrightarrow{\Delta k_{\rho i}}\right) \times \vec{h}_t^*\left(\vec{\rho}\,, \overrightarrow{\Delta k_{\rho i}}\right)\right] \cdot \hat{z} d\vec{\rho}\right\} \quad (14)$$

Aperture Efficiency

The aperture efficiency, η_{ap}, of an absorber under a reflector relates the effective area, A_{eff}, to the physical area, A_{ref}, of the reflector (or of the considered quasi-optical system). This efficiency can be calculated as the ratio between the power absorbed, (14), for broadside incidence, and the power incident to the reflector, $P_{in} = S_i A_{ref}$:

$$\eta_{ap}(f) = \frac{P_{abs}\left(f, \overrightarrow{\Delta k_{\rho i}}=0\right)}{P_{in}} = \frac{A_{eff}}{A_{ref}} \quad (15)$$

As an example, we evaluate this efficiency for the case of the ideal planar absorber described in the previous section but under an optical system. For focusing systems with subtended angles smaller than 20°, i.e. $f_\# > 1.4$, the angular response of the ideal absorber can be considered nearly constant (see Fig. 2). In this case the absorber spatial fields in (12) will resemble the direct fields arriving from the optical system. Thus, the aperture efficiency will be, for an ideal reflector, the well-known spill-over efficiency[2], η_{so}, of the corresponding Airy pattern, except for the cases of electrically small impedance-matched absorbers which are not considered here.

In Fig. 7 the spill-over efficiency, evaluated for normal plane wave incidence on the reflector, versus the size of the ideal absorber, normalized to $\lambda f_\#$, is shown for $f_\# = 2$. When the absorbers would have a non-flat angular response over the reflector subtended angle, the total spatial fields, $\vec{e}^t\left(\vec{\rho}, z = 0, \overrightarrow{\Delta k_{\rho i}}\right)$, will be spatially wider than the direct fields, and therefore, the aperture efficiency would be lower than the spill-over efficiency of the direct fields. This will be also the case when the absorber is not well matched or has a resonant frequency response. Therefore, the use of multi-layer absorbers with stable angular response [45]–[47] will improve the coupling with the optical system, especially for low $f_\#$ optics.

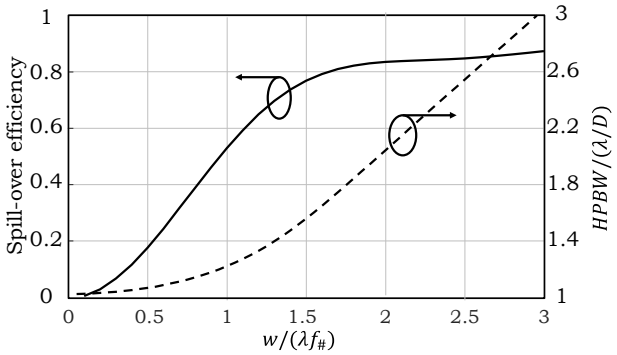

Fig. 7. Spill-over efficiency (solid) and HPBW (dash) for an ideal absorber under an optical system characterized by $f_\# = 2$ and diameter $D = 100\lambda$ versus the physical size of the absorber normalized to $\lambda f_\#$.

Figure 7 also reports the half power beam width (HPBW) normalized to the minimum theoretical HPBW given by a diffraction limited aperture ($HPBW_{min} = \lambda/D$) in the right axis versus the absorber size. It is worth noting that this curve is similar to the one presented in Fig. 4 of [15], since it is presented for a large $f_\#$ and an ideal absorber. The HPBW of the point spread function is a figure of merit for the quality of the generated image. The penalty in terms of system angular beam-width is further quantified in the next sub-section.

Point-Source Angular Response

The angular response of an absorber coupled to an optical system, typically referred as the point spread function in optics, can be evaluated by calculating how much the absorbed power (14) changes versus the impinging plane wave wave-vector $\overrightarrow{\Delta k_{\rho i}}$. A normalized point spread function will be defined here as follows:

$$F(f, \Delta\theta_i, \Delta\phi_i) = \frac{P_{abs}\left(f, \overrightarrow{\Delta k_{\rho i}}\right)}{P_{abs}(f,0)} \quad (16)$$

Thus, the power absorbed can be expressed as:

$$P_{abs}(f, \Delta\theta_i, \Delta\phi_i) = S_i A_{ref} \eta_{ap}(f) F(f, \Delta\theta_i, \Delta\phi_i) \quad (17)$$

To evaluate the angular response in a computationally efficient way, we can use the approximated spatial fields derived in (13). In the case of focusing systems with large $f_\#$, one can neglect the coma term for most of the FO validity

[2] $\eta_{so} \simeq \frac{\iint_A \left(|e_x^d(\vec{\rho})|^2 + |e_y^d(\vec{\rho})|^2\right) d\vec{\rho}}{\iint_\infty \left(|e_x^d(\vec{\rho})|^2 + |e_y^d(\vec{\rho})|^2\right) d\vec{\rho}}$

region. This approximation allows us to evaluate the power absorbed, (14), as a convolution of the spatial Poynting's vector for broadside incidence, ($\overrightarrow{\Delta k}_{\rho i} = 0$), and the absorber domain (square in this case):

$$P_{abs}\left(f, \overrightarrow{\Delta k}_{\rho i}\right) \simeq \frac{1}{2} Re\left\{\iint_{-w/2}^{w/2} \left[\vec{e}_t\left(\vec{\rho} - \overrightarrow{\Delta\rho}_i, 0\right) \times \vec{h}_t^*\left(\vec{\rho} - \overrightarrow{\Delta\rho}_i, 0\right)\right] \cdot \hat{z} d\vec{\rho}\right\} \quad (18)$$

The validity region of (18) is given by (11).

Figure 8(a) shows the angular response of the ideal absorber compared to that of a uniform aperture antenna (inset in Fig. 3) coupled to a parabolic reflector with $f_\# = 2$ for different absorber sizes. It can be noted that, in both cases for physical dimensions small in terms of $\lambda f_\#$, the angular response resembles the well-known Airy distribution. Instead the imager angular response gets much wider when the physical dimension of the absorber increases than in the case of antennas. This implies that, as the absorber size increases, the HPBW increases faster than for a uniform aperture antenna.

This peculiar behavior of the absorbers can be understood if one imagines an absorber large in terms of the wavelength divided in portions having dimension in the order of half wavelength, similarly to the multimode antenna proposed in [20]. Since the power received by each portion sums up almost incoherently, the result is an overall less angular discriminating optical system. For example, Fig. 8(b) shows that for a skewed plane wave incidence, the flash point of the direct field is at the edge of the detecting area. An ideal absorber will receive power proportional to the flux of the Poynting's vector of the direct field, across the entire absorber area, but with maximum contribution from the portion of area at the flash point. On the contrary, an antenna, designed to receive coherently the direct field from broadside, will not receive properly this off-set direct field.

Focusing Efficiency

In Fig. 7 and 8, we have shown that the angular resolution of the imager in Fig. 1 gets worse with increasing dimension of the absorber. To quantify this angular resolution penalty, we now introduce a *focusing efficiency* that relates the solid angle of the Airy pattern, Ω_{Airy} to that of the actual imager angular response, Ω_o, as follows

$$\eta_f = \frac{\Omega_{Airy}}{\Omega_o}. \quad (19)$$

The imager solid angle is defined as follows

$$\Omega_o = \int_0^{2\pi} \int_0^{\frac{\pi}{2}} F(f, \theta, \phi) \sin\theta \, d\theta d\phi, \quad (20)$$

and it is easy to demonstrate that

$$\Omega_{Airy} = \frac{\lambda^2}{A_{ref}}. \quad (21)$$

[3] In the literature, the focusing efficiency for antennas can be referred to utilization efficiency [48], aperture efficiency [49] or taper efficiency [50].

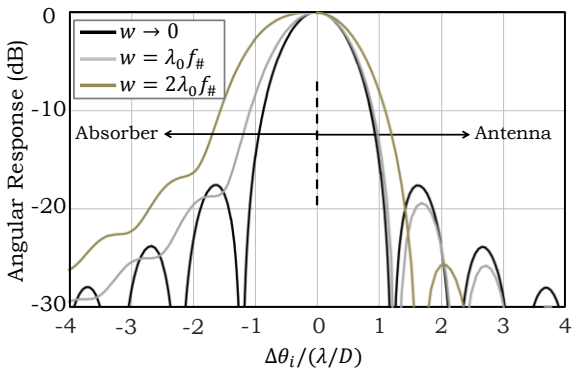

(a)

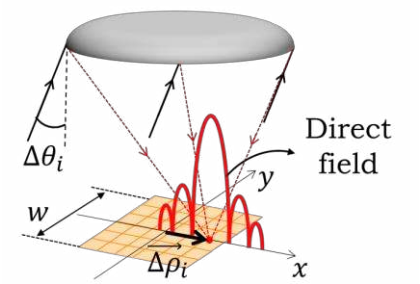

(b)

Fig. 8. (a) Angular response to a plane wave impinging from $\Delta\theta_i$ of both an ideal absorber, and a uniform aperture antenna coupled to a parabolic reflector with $f_\# = 2$. The different curves correspond to several absorber and antenna sizes. (b) Sketch showing the detecting device (antenna/absorber) and direct field for a case of a squinted plane wave incidence.

The focusing efficiency quantifies how much the angular response enlarges with respect to the diffraction limited case. In case of antenna feeds, this efficiency corresponds to the ratio between the achieved directivity in the optical system and the directivity of a uniform circular aperture[3]. In Fig. 9 this efficiency is shown as a function of the absorber size normalized to $\lambda f_\#$ together with the spill-over efficiency for an ideal absorber under a reflector of $f_\# = 2$. It is apparent that for absorbers, the focusing efficiency is much lower than what would be theoretically possible for an antenna with a current distribution that is field matched to the direct field.

The spill-over and focusing efficiencies are commonly used in the antenna reflector community. For comparison, we include in Fig. 9 these efficiencies for a reflector fed by a uniform aperture antenna of side length w (inset in Fig. 3). The spill-over efficiencies (for the antenna calculated as defined in [48]) are nearly the same for both types of feeds, but the focusing efficiency is significantly different. Indeed, except for very small sizes, the antenna type feeds are more directive with respect to a commensurate absorber.

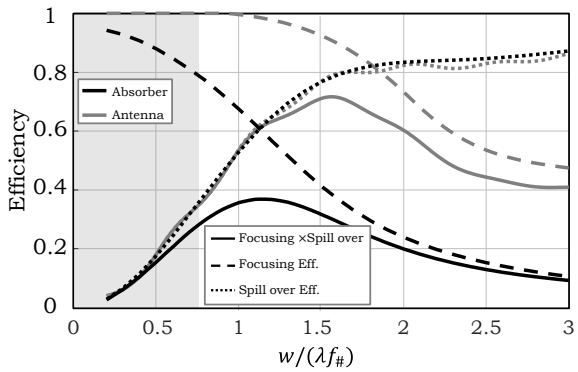

Fig. 9. Focusing and spill-over efficiencies for both ideal antenna and absorbers, with a square dimension of side length w, under a reflector with $f_{\#} = 2$. The grey area indicates the region where the product of the two efficiencies, for the absorber and antenna feeds, are comparable.

To quantify the trade-off between the two different efficiencies in Fig. 9, we also plot the product of these two efficiencies. The maximum value of this product is, in case of absorber feeds, only 37% and it is achieved for $w = 1.2\lambda f_{\#}$, whereas antenna feeds achieved 71% for $w = 1.55\lambda f_{\#}$, thanks to a higher focusing efficiency, which can reach 82% for Gaussian horns [28]. Note, in the case of antennas the product between the spill-over efficiency and the focusing one corresponds to the aperture efficiency [48], except for any other losses in the antenna feed itself. Instead, in the case of absorbers this product is simply a figure of merit that reminds the designer that larger absorbers lead to an inefficient use of the reflector aperture from an angular resolving point of view.

Tightly spaced FPAs of bare absorbers can sometimes be considered the preferred option due to a lower fabrication cost. As it can be seen from Fig. 9, bare absorber FPAs with $w \leq 0.75\lambda f_{\#}$, and focusing efficiencies higher than 80%, have a product of the two key efficiencies comparable to the one of antenna feeds. However, the background noise coming from the box surrounding the absorber should be properly controlled or calibrated, since the absorber has a wide angular response leading to higher sensitivity to undesired sources [15].

The conclusions drawn here can be applied to detectors located close to the focus, where a multi-cascade reflector system can be well modelled with a simplified on-axis parabolic reflector [21]. The achieved spill-over and focusing efficiencies of detectors located far from the focus highly depend on the actual optical system configuration.

V. Distributed-Source Response

The optimization of a densely populated FPA requires to find a suitable trade-off between the sensitivity of each element and the imager resolution. In [15], the optimal FPA architecture that makes use of bare absorbers was studied in the case of background limited noise. Instead, most of the uncooled or medium cooled detectors are limited by the detector noise. In case of bolometric detectors [12], this noise is dependent on the bolometer physical dimensions, w. Therefore, the optimal FPA architecture for these detectors will depend significantly on the aperture and focusing efficiencies, which should accurately be quantified.

The sensitivity of a passive imager can be related to the ability of the system in detecting variations in the temperature of a distributed incoherent source, [15], [51]. Thus, it is related to the power received from a distributed source, P_{abs}^{DS}, with an average temperature, T_s, and angular dimension much larger than the beam of the reflector (imager point spread function).

The received power, P_{abs}^{DS}, over a certain bandwidth $BW = f_2 - f_1$, from incoherent sources operating in Rayleigh Jean's limit with an average temperature, T_s distributed over the full solid angle can be expressed as follows [52]:

$$P_{abs}^{DS} = \int_{f_1}^{f_2} \frac{k_B T_s}{\lambda^2} A_{eff}(f) \int_0^{2\pi} \int_0^{\frac{\pi}{2}} F(f,\theta,\phi) \sin\theta \, d\theta d\phi df \quad (22)$$

where $A_{eff}(f) = \eta_{ap}(f) A_{ref}$ is the effective area of the imager, k_B is the Boltzmann's constant, and $F(f,\theta,\phi)$ is the imager normalized angular response. Equation (22), with the efficiency definitions introduced in Section IV, becomes extremely useful for the design of absorbers. Using the definition in (19), equation (22) can be rewritten as follows

$$P_{abs}^{DS} = k_B T_s \int_{f_1}^{f_2} \frac{\eta_{ap}(f)}{\eta_f(f)} df. \quad (23)$$

This expression is valid for any coupling structure, such as antennas (single or multi-mode) and absorbers. For narrow band systems with bandwidth defined as $BW = f_2 - f_1$, where the integrand in (23) can be approximated constant around the central frequency f_0, one can rewrite (23) as

$$P_{abs}^{DS} \simeq k_B T_s BW \frac{\eta_{ap}(f_0)}{\eta_f(f_0)} \quad (24)$$

In the scientific literature, instead of the ratio $\eta_{ap}(f_0)/\eta_f(f_0)$, one typically finds the normalized throughput, $A_{ref}\Omega_o/\lambda_0^2$, or the number of effective modes, m_{eff}, of the system, [15], [20]. To clarify the discussion for the antenna community, one should consider that for single-mode antennas the aperture efficiency is proportional to the focusing efficiency itself, indeed $\eta_{ap}^{ant} = \eta_{rad}\eta_f$, where η_{rad} is the radiation efficiency [48] (i.e. the ratio between the gain and the directivity in reflectors). Thus, the normalized throughput becomes

$$\frac{A_{ref}\Omega_o}{\lambda_0^2} = \begin{cases} \frac{\eta_{ap}(f_0)}{\eta_f(f_0)} & \text{for absorbers} \\ \eta_{rad}(f_0) & \text{for single-mode antennas} \end{cases} \quad (25)$$

Therefore, for single-mode antennas: $A_{ref}\Omega_A/\lambda_0^2 = \eta_{rad} \leq 1$ and the power received becomes $k_B T_s BW \eta_{rad}$, which is the standard expression in microwave radiometry [52]. Instead, for bare absorber, $A_{ref}\Omega_A/\lambda_0^2$ can be a number much larger than unity. Note that for the case of *Lambert's* absorber without a reflector ($\eta_{ap} = 1$), the absorber's throughput becomes the well-known expression in radiometry [15]: $A_{ref}\Omega_A = \lambda_0^2 \eta_{ap}(f_0)/\eta_f(f_0) = \pi A_{ref}$.

The term $\eta_{ap}(f_0)/\eta_f(f_0)$ is plotted in Fig. 10 for the case of an ideal absorber under a parabolic reflector with $f_{\#} = 2$. The

normalized throughput $A_{ref}\Omega_o/\lambda_0^2$, derived accordingly to [15] by using Airy pattern considerations, is also reported in Fig. 10. The agreement is very good since the calculations were done for an ideal absorber under a large $f_\#$ parabolic reflector. However, the analysis proposed in this paper can accurately quantify the normalized throughput for many other cases such as optics with small $f_\#$ (common in integrated lenses [5]), absorbers with a non-flat angular response [9], or even resonant absorbers [7], [8], [30]. As an example, Fig. 10 also shows the normalized throughput for an ideal absorber under a $f_\# = 0.6$ parabolic reflector. In such case, its value differs significantly from the one calculated with the Airy pattern formula [15], leading to a lower power received from a distributed incoherent source and, therefore, lower sensitivity.

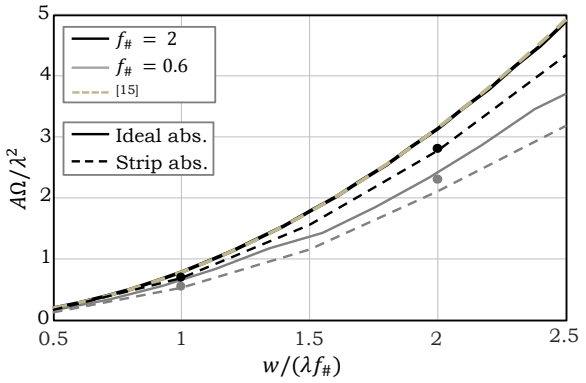

Fig. 10. Normalized throughput calculated as η_{ap}/η_f versus the absorber size, w, for two optical systems with $f_\# = 0.6$ (grey) and $f_\# = 2$ (black). The solid lines are related to the ideal absorbers, the dashed lines to an absorber based on resistive strips, and the dots to the relevant performed full wave simulations.

VI. Numerical Examples

In this section, the results calculated with the proposed methodology are compared with those obtained by using full wave simulations. An absorber made of linear resistive strips above a $\lambda/4$ back reflector is considered as a test case. For this case a reference analytical circuit is available in [42]. The absorber is composed of resistive mesh strips with a surface resistance of $R_s = 10\ \Omega/\square$ and width of 2.7 μm. The strips have a periodicity of $d_y = 102$ μm, and back short distance of $h_{bs} = 150$ μm. The total dimension of the absorber is $w \times w$ (Fig. 1). The operating frequency for this example is 500 GHz.

Large $f_\#$ Optics

As described in the previous section, the angular response for absorbers under a large $f_\#$ optical system, according to (18), is basically the convolution of the total field with the spatial domain of the absorber. In such a case, when the absorber can be considered ideal, the throughput can be evaluated using Airy pattern considerations as in [15]. The plane wave response of the considered absorber is shown in Fig. 2, showing similar angular response to the ideal absorber. The absorbed power has been evaluated by using the equivalent circuit proposed in [42], as well as the generic circuit for an arbitrary absorber shape described in the Appendix.

In Figs. 11(a) and (b) the power absorbed by the linear strip mesh, placed under a parabolic reflector with $f_\# = 2$ and diameter $D = 100\lambda$, is shown versus the plane wave angle of incidence, for two different physical dimensions of the absorber (the absorber is made of 7 and 14 resistive strips for the $w = 2\lambda$ and $w = 4\lambda$ cases, respectively). The incident plane wave is assumed having amplitude $|E_0| = 1\ \mathrm{V/m}$ and polarization along x. The results are compared with those carried out by using full wave simulations. Specifically, first the direct field focalized by the reflector on a square area at a z-quote above the absorber (Fig. 12) is evaluated by using the Physical Optics solver of GRASP. Then, the field is used as an external source in CST MS to compute the power dissipated into the resistive strips. Since the procedure has to be repeated for each angle of the plane wave impinging on the reflector, $\Delta\theta_i$, the computation of the angular response via the full wave (FW) simulations is time-consuming, and for this reason the results are reported only for a limited number of incident angles. On the contrary, the FO spectral method takes a few minutes for obtaining an accurate 2D angular response of the imager. The agreement between both methods is excellent.

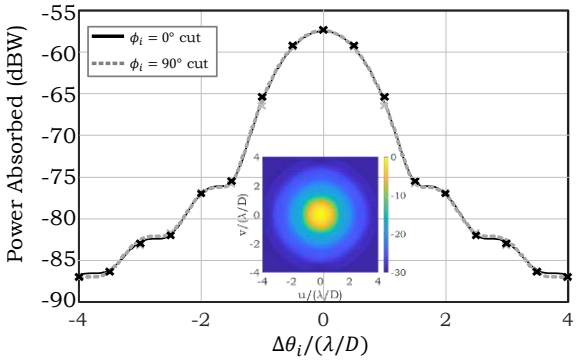

(a)

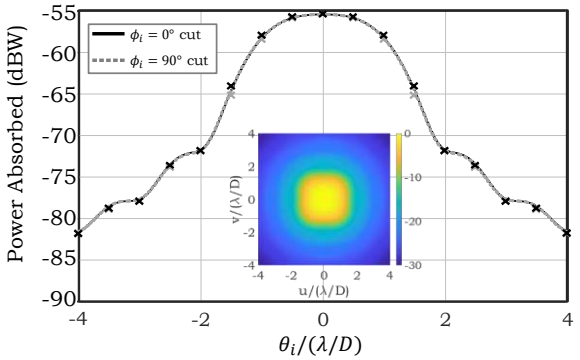

(b)

Fig. 11. Power absorbed versus the plane wave incident angle (non-normalized angular response) of a linear strip absorber with side length w coupled to a reflector with $f_\# = 2$: (a) $w = \lambda f_\#$ and (b) $w = 2\lambda f_\#$. Solid lines: calculated by using (18). Cross marks: obtained via full wave simulations. The inset illustrates the 2D response in u-v coordinates

The aperture and the focusing efficiencies of a strip absorber under a $f_\# = 2$ parabolic reflector can be estimated by using both the FO and FW approaches. Results are summarized in Table I, showing excellent agreement. Normalized throughputs can also be estimated for the cases given in Table I by using (25). The aperture efficiencies are slightly lower than those

related to the ideal absorber (Fig. 9), due to the fact that the strip mesh structure presents a small mismatch with the incoming waves. In particular, the imaginary part of the strip absorbers presents an inductive behavior, that leads to only 93% absorption of the impinging power, for broadside plane wave illumination as shown in Fig. 2. The focusing efficiencies are instead comparable. Therefore, the normalized throughput is slightly lower than the one of the ideal absorber (Fig. 10).

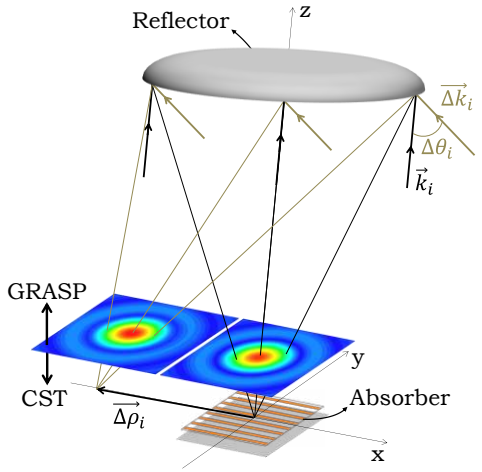

Fig. 12. A schematic representation of the geometry under discussion and of the GRASP + CST full wave simulation procedure. The direct field is obtained by GRASP and then used as an external source in CST.

TABLE I
COMPARISON OF EFFICIENCIES FOR STRIP ABSORBER $f_\# = 2$

	Fourier Optics	Full Wave
$w = \lambda f_\#$	$\eta_{ap} = 48\%$ $\eta_f = 70\%$ $A\Omega/\lambda^2 = 0.7$	$\eta_{ap} = 49\%$ $\eta_f = 70\%$ $A\Omega/\lambda^2 = 0.7$
$w = 2\lambda f_\#$	$\eta_{ap} = 76\%$ $\eta_f = 27\%$ $A\Omega/\lambda^2 = 2.8$	$\eta_{ap} = 77\%$ $\eta_f = 27\%$ $A\Omega/\lambda^2 = 2.8$

Small $f_\#$ Optics

The lower is the $f_\#$, the more difficult is to evaluate the performances of absorbers under optical systems. Firstly, the absorber angular response cannot be approximated by a convolution with the broadside total field since the shape of the direct field changes significantly even for an incident angle of a couple of HPBWs due to the coma phase term (Fig. 6). Secondly, the absorber plane wave response can affect significantly the shape of the total spatial fields. Thirdly, the absorber's overall physical dimension can be comparable to the wavelength, or even smaller, making the FO + Floquet mode approach not applicable.

The calculated angular response of a strip absorber of $2\lambda f_\#$ (7 strips) in side length under a reflector with $f_\# = 0.6$ is shown in Fig. 13(b), and compared with full wave simulations. The agreement is very good even if the absorber is only $1.2\lambda \times 1.2\lambda$. The full wave absorbed power is slightly higher in the $\phi_i = 0°$ cut, which can be associated with edge effects due to the finiteness of the strips. Smaller absorber dimensions, such as the case show in Fig. 13(a) (absorber with a $w = 0.6\lambda$ and only 3 strips), will lead to larger discrepancies between the FO and FW simulations. Indeed, in such case the absorber effective area is larger than the physical one as shown in Fig. 3, and the edge effects are even more significant. Despite this, the agreement with full wave simulations is still quite good as shown in Fig. 13(a) for both a finite and an infinite back short.

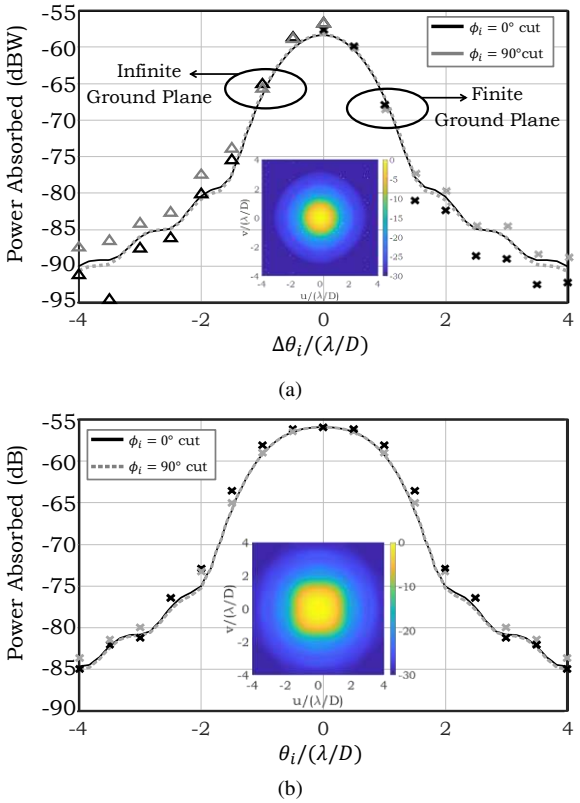

Fig. 13. Power absorbed versus the plane wave incident angle (non-normalized angular response) of a linear strip absorber with side length w coupled to a reflector with $f_\# = 0.6$: (a) $w = \lambda f_\#$ and (b) $w = 2\lambda f_\#$. Solid lines: calculated by using (14). Marks: obtained via full wave simulations. The inset illustrates the 2D response in u-v coordinates

The values of the simulated aperture and focusing efficiencies are summarized in Table II for both absorber dimensions. The FW simulated focusing efficiencies are about 10% different in both cases due to the edge effects, whereas the aperture efficiency of the smallest case ($w = \lambda f_\#$) is 15% higher than predicted with the FO tool due to a larger effective area than the physical one. The values of the aperture efficiency for both cases are lower than the values given for large $f_\#$, due to the variation of the absorber response to the incident plane waves, as shown in Fig. 2; instead, the focusing efficiency is higher than the cases shown in Table I, because of the coma distortion in the direct field.

In Fig. 10 the estimated values for the normalized throughputs in case of the linear resistive mesh are also shown for the two considered reflectors, using both the FO approach and the FW simulations. The values obtained for all cases are lower than the ones estimated in [15]. It can be noted that for some cases the absorber receives up to 40% less power than the one estimated in [15], leading to a less sensitive instrument.

TABLE II
COMPARISON OF EFFICIENCIES FOR STRIP ABSORBER $f_{\#} = 0.6$

	Fourier Optics	Full Wave
$w = \lambda f_{\#}$	$\eta_{ap} = 40\%$ $\eta_f = 74\%$ $A\Omega/\lambda^2 = 0.53$	$\eta_{ap} = 46\%$ $\eta_f = 82\%$ $A\Omega/\lambda^2 = 0.56$
$w = 2\lambda f_{\#}$	$\eta_{ap} = 68\%$ $\eta_f = 32\%$ $A\Omega/\lambda^2 = 2.1$	$\eta_{ap} = 67\%$ $\eta_f = 29\%$ $A\Omega/\lambda^2 = 2.3$

VII. CONCLUSION

Passive imaging cameras at sub-millimeter wavelengths are being developed by using bare absorbing meshes without any antenna coupling (lens or horn) structures in the focal plane of a focusing system. The design of such arrays is typically done resorting to geometrical considerations or basic broadside plane wave incidence analysis. This work presents a spectral electromagnetic model that is based on linking a Plane Wave Spectral representation of the direct field focused by the optical system with a Floquet Wave representation of the field in the absorbing mesh. The results obtained by the present model have been compared, with excellent agreement, with those obtained by full wave simulations. Thus, the proposed spectral method provides an accurate and efficient way to estimate the key optical properties of the imager inside the region of validity of the Fourier Optics.

The most important design aspect that emerges from the present study of focusing systems in reception is associated with the introduction of the intuitive focusing efficiency parameter. This parameter leads to two important conclusions. Firstly, when comparing bare absorber FPAs and antenna feeds of equivalent dimensions, the latter leads to higher focusing efficiencies, and therefore better imaging resolution. Only very tightly sampled absorber based FPAs lead to a comparable trade-off in terms of received power and angular resolution, when compared to antenna based FPAs. Secondly, while for antennas it is well known that the power received from a distributed incoherent source is $P_{ant}^{DS} = \eta_{rad} k_b T_s BW$, for absorber based FPAs, the corresponding received power is typically quantified introducing an effective number of modes: $P_{abs}^{DS} = m_{eff} \times k_b T_s BW$. Here, it is shown that the effective number of modes m_{eff} can be conveniently evaluated as the ratio between the aperture, η_{ap}, and the focusing efficiency, η_f.

APPENDIX:
CIRCUIT FIELD REPRESENTATION FOR OPTICS COUPLED PLANAR ABSORBERS

The field in the surrounding of a periodic absorber coupled to an optical system can be expressed as a coherent summation of the absorber response to each plane wave coming from the optical system. The spectral response of the absorber to a plane wave can be modeled by using the fundamental Floquet mode field representation, neglecting any finiteness effect, and assuming a periodicity less than half wavelength, i.e. $d_{x/y} < \lambda/2$.

In general, any periodic planar structure can be modelled by using the equivalent network shown in Fig. A1, where the TE and TM transmission lines represent the propagation of the respective fundamental Floquet modes having characteristic impedances $Z_0^{TE}(k_\rho) = \zeta_0 k_0/k_z$ and $Z_0^{TM}(k_\rho) = \zeta_0 k_z/k_0$, respectively, where $k_z = \sqrt{k_0^2 - k_\rho^2}$. The matrix

$$\bar{Y}_{abs}(k_\rho) = \begin{bmatrix} Y_{abs}^{TETE}(k_\rho) & Y_{abs}^{TETM}(k_\rho) \\ Y_{abs}^{TMTE}(k_\rho) & Y_{abs}^{TMTM}(k_\rho) \end{bmatrix}$$

represents the absorbers response to the TE and TM plane wave excitations.

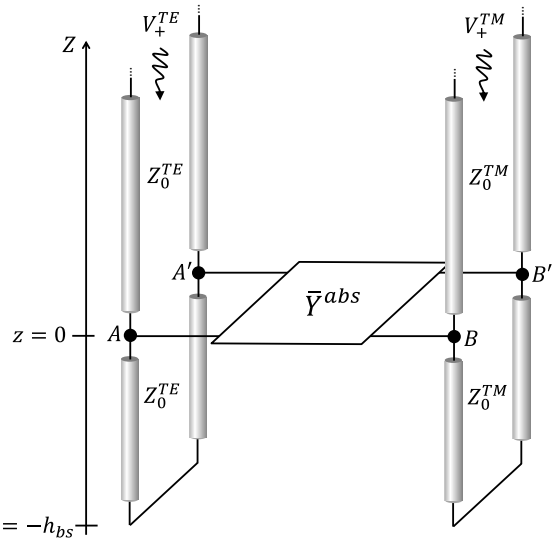

Fig. A1. Equivalent transmission line model of a periodic absorber with period smaller than half wavelength under a certain incident plane wave, $\vec{k}_\rho$.

For a periodic structure placed at the focal plane of an optical system, the voltage sources in the Floquet equivalent network are related to the PWS of the direct field coming from the optical system, (3). They can be evaluated as:

$$V_+^{TM}(\vec{k}_\rho) = \sqrt{d_x d_y} E_\theta^d(\vec{k}_\rho) \frac{k_z}{k_0} \quad \text{(A.1)}$$

$$V_+^{TE}(\vec{k}_\rho) = \sqrt{d_x d_y} E_\phi^d(\vec{k}_\rho) \quad \text{(A.2)}$$

where d_x and d_y are the periods of the array along x and y, respectively; and $E_\theta^d(\vec{k}_\rho)$ and $E_\phi^d(\vec{k}_\rho)$ are the θ- and ϕ- spectral components of the direct field as given in (3) and (4).

By using the scattering parameters representation of the structure, one can evaluate the current flowing, $I^{TE/TM}(\vec{k}_\rho, z)$, and voltage drop, $V^{TE/TM}(\vec{k}_\rho, z)$, at the transmission line quote above the absorber as follows:

$$V^{TE/TM}(\vec{k}_\rho, 0^+) = V_+^{TE/TM} + V_-^{TE/TM} \quad \text{(A.3)}$$

$$I^{TE/TM}(\vec{k}_\rho, 0^+) = \frac{1}{Z_0^{TE/TM}}\left(V_+^{TE/TM} - V_-^{TE/TM}\right) \quad \text{(A.4)}$$

where $\begin{bmatrix} V_-^{TE} \\ V_-^{TM} \end{bmatrix} = \bar{S}(k_\rho) \begin{bmatrix} V_+^{TE} \\ V_+^{TM} \end{bmatrix}$ are the reflected voltages at AA'/BB' terminal, since $\bar{S}(k_\rho) = \begin{bmatrix} S^{TETE}(k_\rho) & S^{TETM}(k_\rho) \\ S^{TMTE}(k_\rho) & S^{TMTM}(k_\rho) \end{bmatrix}$

represents the scattering matrix of the transmission line at $z = 0^+$ quote.

The averaged magnetic and electric spectral fields over the absorber unit cell can be derived as follows:

$$E^t_{k_\rho}(\vec{k}_\rho, z) = \frac{1}{\sqrt{d_x d_y}} V^{TM}(\vec{k}_\rho, z) \quad (A.5)$$

$$E^t_{\phi}(\vec{k}_\rho, z) = \frac{1}{\sqrt{d_x d_y}} V^{TE}(\vec{k}_\rho, z) \quad (A.6)$$

$$H^t_{k_\rho}(\vec{k}_\rho, z) = -\frac{1}{\sqrt{d_x d_y}} I^{TE}(\vec{k}_\rho, z) \quad (A.7)$$

$$H^t_{\phi}(\vec{k}_\rho) = \frac{1}{\sqrt{d_x d_y}} I^{TM}(\vec{k}_\rho, z) \quad (A.8)$$

Combining expressions (A.5)–(A.8) one can express the average electric and magnetic spectral fields in Cartesian coordinates as:

$$\begin{bmatrix} E^t_x(\vec{k}_\rho, z) \\ H^t_x(\vec{k}_\rho, z) \end{bmatrix} = \begin{bmatrix} E^t_{k_\rho}(\vec{k}_\rho, z) \\ H^t_{k_\rho}(\vec{k}_\rho, z) \end{bmatrix} (\hat{k}_\rho \cdot \hat{x}) + \begin{bmatrix} E^t_{\phi}(\vec{k}_\rho, z) \\ H^t_{\phi}(\vec{k}_\rho, z) \end{bmatrix} (\hat{\phi} \cdot \hat{x}) \quad (A.9)$$

$$\begin{bmatrix} E^t_y(\vec{k}_\rho, z) \\ H^t_y(\vec{k}_\rho, z) \end{bmatrix} = \begin{bmatrix} E^t_{k_\rho}(\vec{k}_\rho, z) \\ H^t_{k_\rho}(\vec{k}_\rho, z) \end{bmatrix} (\hat{k}_\rho \cdot \hat{y}) + \begin{bmatrix} E^t_{\phi}(\vec{k}_\rho, z) \\ H^t_{\phi}(\vec{k}_\rho, z) \end{bmatrix} (\hat{\phi} \cdot \hat{y}) \quad (A.10)$$

REFERENCES

[1] R. Appleby and H. Wallace, "Standoff detection of weapons and contraband in the 100 GHz to 1 THz region," *IEEE Trans. on Antennas and Propag.*, vol. 55, no. 11, pp. 2944–2956 Nov. 2007.

[2] E. Grossman, C. Dietlein, J. Ala-Laurinaho, M. Leivo, L. Gronberg, M. Gronholm, P. Lappalainen, A. Rautiainen, A. Tamminen, and A. Luukanen, "Passive terahertz camera for standoff security screening," *Appl. Opt.*, vol. 49, pp. E106–E120, Jul. 2010.

[3] K. B. Cooper, R. J. Dengler, N. Llombart, B. Thomas, G. Chattopadhyay, and P. H. Siegel, "THz imaging radar for standoff personnel screening," *IEEE THz Sci. and Technol.*, vol. 1, no. 1, pp. 169–182, Sept. 2011.

[4] E. Heinz, T. May, D. Born, G. Zieger, K. Peiselt, V. Zakosarenko, T. Krause, A. Krüger, M. Schulz, F. Bauer, and H.-G. Meyer, "Progress in passive submillimeter-wave video imaging," *Proc. SPIE*, June 2014.

[5] G. J. Stacey et. al, "SWCam: the short wavelength camera for the CCAT observatory," *Proc. SPIE vol. 9153, Millimeter, Submillimeter, and Far-Infrared Detectors and Instrumentation for Astronomy VII*, Aug. 2014.

[6] J. J. A Baselmans, J. Bueno, S. J. C. Yates, O. Yurduseven, N. Llombart, K. Karatsu, A. M. Baryshev, L. Ferrari, A. Endo, D. J. Thoen, P. J. de Visser, R. M. J. Janssen, V. Murugesan, E. F. C. Driessen, G. Coiffard, J. Martin-Pintado, P. Hargrave, and M. Griffin, "A kilo-pixel imaging system for future space based far-infrared observatories using microwave kinetic inductance detectors," *Astron. and & Astrphys. ArXiv e-prints*, vol. 601, Sept. 2016.

[7] M. Calvo, A. Benoît, A. Catalano, et al, "The NIKA2 instrument, a dual-band kilopixel KID array for millimetric astronomy," *J. of Low Temp. Phys.*, vol. 184, no. 3–4, pp. 816–823, Jul. 2016.

[8] S. Rowe, E. Pascale, S. Doyle, C. Dunscombe, P. Hargrave, A. Papageorgio, K. Wood, P. A. R. Ade, P. Barry, A. Bideaud, T. Brien, C. Dodd, W. Grainger, J. House, P. Mauskopf, P. Moseley, L. Spencer, R. Sudiwala, C. Tucker, and I. Walker, "A passive terahertz video camera based on lumped element kinetic inductance detectors," *Rev. of Sci. Inst.,* vol. 87, no. 3, Mar. 2016.

[9] A. Timofeev, J. Luomahaara, L. Grönberg, A. Mäyrä, H. Sipola, M. Aikio, M. Metso, V. Vesterinen, K. Tappura, J. Ala-Laurinaho, A. Luukanen, and J. Hassel, "Optical and electrical characterization of a large kinetic inductance bolometer focal plane array," *IEEE THz Sci. and Technol,* vol. 7, no. 2, pp. 218–224, Mar. 2017.

[10] N. Oda, S. Kurashina, M. Miyoshi, K. Doi, T. Ishi, T. Sudou, T. Morimoto, H. Goto, and T. Sasaki, "Microbolometer terahertz focal plane array and camera with improved sensitivity in the sub-terahertz region," *J. of Infrared, Millimeter, and THz Waves*, vol. 36, no. 10, pp. 947–960, Oct. 2015.

[11] F. Sakran, Y. Neve-Oz, A. Ron, M. Golosovsky, D. Davidov and A. Frenkel, "Absorbing frequency-selective-surface for the mm-wave range," *IEEE Trans. on Antennas and Propag.,* vol. 56, no. 8, pp. 2649–2655, Aug. 2008.

[12] P. L. Richards, "Bolometers for infrared and millimeter waves," *J. of Appl. Phys.*, vol. 76, no. 1, pp. 1–24, Mar. 1994.

[13] T. H. Buttgenbach, "An improved solution for integrated array optics in quasi-optical mm and submm receivers: the hybrid antenna," *IEEE Trans. Microw. Theory and Techn.*, vol. 41, no. 10, pp. 1750–1760, Oct. 1993.

[14] G. M. Rebeiz, L. P. B. Katehi, W. Y. Ali-Ahmad, G. V. Eleftheriades, and C. C. Ling, "Integrated horn antennas for millimeter-wave applications," *IEEE Antennas Propag. Mag.*, vol. 34, pp. 7–16, Feb. 1992.

[15] M. J. Griffin, J. J. Bock, and W. K. Gear, "Relative performance of filled and feedhorn-coupled focal-plane architectures," *Appl. Opt.*, vol. 41, no. 31, pp. 6543–6554, Nov. 2002.

[16] C. Thomas and S. Withington, "Optical modeling techniques for multimode horn-coupled power detectors for submillimeter and far-infrared astronomy," *J. of the Opt. Society of America A*, vol. 30, no. 8, pp. 1703–1713, Aug. 2013.

[17] D. McCarthy, et. al, "Optical characterisation and analysis of multi-mode pixels for use in future far infrared telescopes", *Proc. SPIE 9914, Millimeter, Submillimeter, and Far-Infrared Detectors and Instrumentation for Astronomy VIII*, Jul. 2016.

[18] J. F. Johansson, "Millimeter-wave imaging theory and experiments," *Onsala Space Observatory Research Report*, No. 151, vol. 1, p. 1, 1986.

[19] S. Rao, L. Shafai, and S. K. Sharma, Ed., *Handbook of Reflector Antennas and Feed Systems Volume II*, Artech House, 2013.

[20] D. Rutledge, and S. Schwarz, "Planar multimode detector arrays for infrared and millimeter-wave applications," *IEEE J. of Quantum Elec,*, vol. 17, no. 3, pp. 407–414, Mar. 1981.

[21] W. V. T. Rusch, A. Prata, Y. Rahmat-Samii, and R. A. Shore, "Derivation and application of the equivalent paraboloid for classical offset Cassegrain and Gregorian antennas," *IEEE Trans. on Antennas and Propag.*, vol. 38, no. 8, pp. 1141–1149, Aug. 1990.

[22] B. Veidt, and P. Dewdney, "Bandwidth limits of beamforming networks for low-noise focal-plane arrays," *IEEE Trans. on Antennas and Propag.*, vol. 53, no. 1, pp. 450–454, Jan. 2005.

[23] J. Diao, and K. F. Warnick, "On the bandwidth gap between the array-feed and cluster-feed regimes for broadband multifeed systems," *IEEE Trans. on Antennas and Propag.*, vol. 64, no. 6, pp. 2207–2216, June 2016.

[24] E. Wolf, "Electromagnetic diffraction in optical systems. I. an integral representation of the image field," in *Proceedings of the Royal Society of London. Series A. Mathematical and Physical Sciences*, vol. 253, no. 1274, pp. 349–357, 1959.

[25] N. Llombart, B. Blázquez, A. Freni, and A. Neto, "Fourier optics for the analysis of distributed absorbers under THz focusing systems," *IEEE Trans. THz Sci. and Technol.*, vol. 5, no. 4, pp. 573–583, July 2015.

[26] X. Gao, and Z. Du, "Modelling of a paraboloid antenna for receiving and its equivalent circuit," *IET Microw., Antennas & Propag.*, vol. 8, no. 12, pp. 931–936, Sept. 2014.

[27] V. Rumsey, "On the design and performance of feeds for correcting spherical aberration," *IEEE Trans. on Antennas and Propag.*, vol. 18, no. 3, pp. 343–351, May 1970.

[28] P. F. Goldsmith, *Quasioptical Systems: Gaussian Beam Quasioptical Propagation and Applications*, Wiley-IEEE Press, pp. 129–133, 1997.

[29] G. Rieke, *Detection of Light: From the Ultraviolet to the Submillimeter* Cambridge, Cambridge Univ. Press, 2003, 2nd ed., pp. 287–288, 2002.

[30] S. O. Dabironezare, E. Gandini, J. Hassel, A. Neto, and N. Llombart, "Design of a dual-band FSS based bolometer for security imagers at THz frequencies," *European conference on Antennas and Propagation*, Davos, Switzerland, Apr. 2016.

[31] R. L. Fante, and M. T. McCormack, "Reflection properties of the Salisbury screen," *IEEE Trans. on Antennas and Propag.*, vol. 36, no. 10, pp. 1443–1454, Oct. 1988.

[32] F. Gross, and E. Kuster, "An optimized polarization sensitive Salisbury screen," *IEEE Trans. on Antennas and Propag.*, vol. 35, no. 12, pp. 1492–1495, Dec. 1987.

[33] CST Microwave Studio, CST [Online]. Available: http://www.cst.com/.

[34] A. Nagamune, and P. H. Pathak, "An efficient plane wave spectral analysis to predict the focal region fields of parabolic reflector antennas for small and wide angle scanning," *IEEE Trans. on Antennas and Propag.*, vol. 38, no. 11, pp. 1746–1756, Nov. 1990.
[35] F. Costa, A. Monorchio, and G. Manara, "Analysis and design of ultra-thin electromagnetic absorbers comprising resistively loaded high impedance surfaces," *IEEE Trans. on Antennas and Propag.*, vol. 58, no. 5, pp. 1551–1558, May 2010.
[36] G. A. Deschamps, "Ray techniques in electromagnetics," *Proc. of the IEEE*, vol. 60, no. 9, pp. 1022–1035, Sept. 1972.
[37] S. von Hoerner, "Strong coma lobes from small gravitational deformations," *IEEE Trans. on Antennas and Propag.*, vol. 28, no. 5, pp. 652–657, Sept.1980.
[38] C. Dragone, "A first-order treatment of aberrations in Cassegrainian and Gregorian antennas," *IEEE Trans. on Antennas and Propag.*, vol. 30, no. 3, pp. 331–339, May 1982.
[39] J. Ruze, "Lateral-feed displacement in a paraboloid," *IEEE Trans. Antennas and Propag.*, vol. 13, no. 5, pp. 660–665, Sept. 1965.
[40] R. Hansen, *Microwave Scanning Antennas. Volume 1: Apertures*, Academic Press, pp. 139–143, 1964.
[41] "GRASP Software," TICRA, Copenhagen, Denmark.
[42] B. Blázquez, N. Llombart, D. Cavallo, A. Freni, and A. Neto, "A rigorous equivalent network for linearly polarized THz absorbers," *IEEE Trans. on Antennas and Propag.*, vol. 62, no. 10, pp. 5077–5088, Oct. 2014.
[43] D. Cavallo, W. H. Syed, and A. Neto, "Closed-form analysis of artificial dielectric layers—part I: properties of a single layer under plane-wave incidence," *IEEE Trans. on Antennas and Propag.*, vol. 62, no. 12, pp. 6256–6264, Dec. 2014.
[44] S. Maci, M. Caiazzo, A. Cucini, and M. Casaletti, "A pole-zero matching method for EBG surfaces composed of a dipole FSS printed on a grounded dielectric slab," *IEEE Trans. on Antennas and Propag.*, vol. 53, no. 1, pp. 70–81, Jan. 2005.
[45] A. Kazemzadeh, and A. Karlsson, "Multilayered wideband absorbers for oblique angle of incidence," *IEEE Trans. on Antennas and Propag.*, vol. 58, no. 11, pp. 3637–3646, Nov. 2010.
[46] G. I. Kiani, K. L. Ford, K. P. Esselle, A. R. Weily, and C. J. Panagamuwa, "Oblique incidence performance of a novel frequency selective Surface absorber," *IEEE Trans. on Antennas and Propag.*, vol. 55, no. 10, pp. 2931–2934, Oct. 2007.
[47] W. Tang, G. Goussetis, H. Legay, and N. J. G. Fonseca, "Oblique efficient synthesis of low-profile angularly-stable and polarization-independent frequency-selective absorbers with a reflection band" *IEEE Trans. on Antennas and Propag.*, vol. 63, no. 2, pp. 621–629, Feb. 2015.
[48] J. D. Kraus, *Antennas for all applications*, 2nd edition, Tata McGraw-Hill, pp. 573–587, 1997.
[49] R. E. Collin, *Antennas and Radiowave propagation*, McGraw Hill, Chapter 4, 1985.
[50] W. L. Stutzman and G.A. Thiele, *Antenna Theory and Design,* John Willey & Sons, Chapter 8, 1981.
[51] S. L. van Berkel, O. Yurduseven, A. Freni, A. Neto, and N. Llombart, "THz imaging using uncooled wideband direct detection focal plane arrays," *IEEE Trans. THz Sci. and Technol.*, vol. 7, no. 5, pp. 481–492, Sept. 2017.
[52] David Long, Fawwaz T. Ulaby, *Microwave Radar and Radiometric Remote Sensing,* Artech House, Chapter 6, 2015.

Nuria Llombart (S'06–M'07–SM'13) received the Master's degree in electrical engineering and Ph.D. degrees from the Polytechnic University of Valencia, Valencia, Spain, in 2002 and 2006, respectively.

During her Master's degree studies, she spent one year at the Friedrich-Alexander University of Erlangen-Nuremberg, Erlangen, Germany, and worked at the Fraunhofer Institute for Integrated Circuits, Erlangen, Germany. From 2002 to 2007, she was with the Antenna Group, TNO Defense, Security and Safety Institute, The Hague, The Netherlands, working as a Ph.D. student and afterwards as a Researcher. From 2007 to 2010, she was a Postdoctoral Fellow with the California Institute of Technology, working with the Submillimeter Wave Advance Technology Group, Jet Propulsion Laboratory, Pasadena, CA, USA. She was a "Ramón y Cajal" fellow in the Optics Department, Complutense University of Madrid, Madrid, Spain, from 2010 to 2012. In September 2012, she joined the THz Sensing Group, Technical University of Delft, Delft, The Netherlands, where as of February 2018 she is a Full Professor. She has coauthored more than 150 journal and international conference contributions. Her research interests include the analysis and design of planar antennas, periodic structures, reflector antennas, lens antennas, and waveguide structures, with emphasis in the THz range.

Dr. Llombart was the recipient H. A. Wheeler Award for the Best Applications Paper of 2008 in the IEEE TRANSACTIONS ON ANTENNAS AND PROPAGATION, the 2014 THz Science and Technology Best Paper Award of the IEEE Microwave Theory and Techniques Society, and several NASA awards. She was also the recipient of the 2014 IEEE Antenna and Propagation Society Lot Shafai Mid-Career Distinguished Achievement Award. She serves as a Board member of the IRMMW-THz International Society. In 2015, she was the recipient of European Research Council Starting Grant.

Shahab Oddin Dabironezare (S'11) received the B.Sc. degrees (*cum laude*) from Ferdowsi University of Mashhad (FUM), and M.Sc. degree from the Delft University of Technology (TU Delft), in electrical engineering in 2013 and 2015, respectively. He is currently pursuing the Ph.D. degree in Terahertz Sensing Group, TU Delft.

His research interests include quasi-optical systems, analytical/numerical techniques in electromagnetics, passive imaging systems, and wideband antenna designs for millimeter and submillimeter-wave applications.

Giorgio Carluccio was born in 1979 and grew up in Ortelle, Italy. He received the Laurea degree in telecommunications engineering and the Ph.D. degree in information engineering from the University of Siena, Siena, Italy, in 2006 and 2010, respectively.

In 2008 and 2009 he was an Invited Visiting Scholar with the ElectroScience Laboratory, Department of Electrical and Computer Engineering, The Ohio State University, Columbus, Ohio, USA. From 2010 to 2012 and from 2013 to 2014, he was a Post-Doctoral Research Associate with the Department of Information Engineering and Mathematics, University of Siena. From 2012 to 2013, he was a Post-Doctoral Research Associate with the Department of Electronics and Telecommunication, University of Florence, Florence, Italy. In 2012 and 2013 he was a Visiting Post-Doctoral Researcher with the Department

of Microelectronics, Delft University of Technology (TU Delft), Delft, The Netherlands, where he also was a Post-Doctoral Researcher from 2014 to 2018. Since 2018 he has been a RF circuit and antenna scientist with NXP Semiconductor, Eindhoven, The Netherlands, where he works on antenna-in-package devices for automotive radar applications. His research interests deal with electromagnetic wave theory, mainly focused on asymptotic high-frequency techniques for electromagnetic scattering and propagation; and with modeling and design of antennas: mainly, dielectric lens antennas, reflector array antennas, and THz antennas based on photoconductive materials.

Dr. Carluccio was the recipient of the 2018 EurAAP International "Leopold B. Felsen Award for Excellence in Electrodynamics", and of the 2010 URSI Commission B Young Scientist Award at the International Symposium on Electromagnetic Theory (EMTS 2010), where he also received the third prize for the Young Scientist Best Paper Award.

Angelo Freni (S'90–M'91–SM'03) received the Laurea (Doctors) degree in electronics engineering from the University of Florence, Florence, Italy, in 1987.

Since 1990, he has been with the Department of Electronic Engineering, University of Florence, first as an Assistant Professor and, since 2002, as an Associate Professor of electromagnetism. From 1995 to 1999, he has also been an Adjunct Professor with the University of Pisa, Pisa, Italy, and since 2010, a Visiting Professor with the TU Delft University of Technology, Delft, The Netherlands. During 1994, he was involved in research with the Engineering Department, University of Cambridge, Cambridge, U.K., concerning the extension and the application of the finite element method to the electromagnetic scattering from periodic structures. From 2009 to 2010, he also spent one year as a Researcher with the TNO Defence, Security and Safety, The Hague, The Netherlands, where he was involved with the electromagnetic modeling of kinetic inductance devices and their coupling with array of slots in the THz range. His research interests include meteorological radar systems, radiowave propagation, numerical and asymptotic methods in electromagnetic scattering and antenna problems, electromagnetic interaction with moving media, and remote sensing. In particular, part of his research concerned numerical techniques based on the integral equation with a focus on domain-decomposition and fast solution methods.

Andrea Neto (M'00–SM'10–F'16) received the Laurea degree (summa cum laude) in electronic engineering from the University of Florence, Florence, Italy, in 1994, and the Ph.D. degree in electromagnetics from the University of Siena, Siena, Italy, in 2000. Part of his Ph.D. degree was developed at the European Space Agency Research and Technology Center Noordwijk, The Netherlands.

He worked for the Antenna Section at the European Space Agency Research and Technology Center for over two years. From 2000 to 2001, he was a Postdoctoral Researcher with the California Institute of Technology, Pasadena, CA, USA, where he worked with the Sub-mm Wave Advanced Technology Group. From 2002 to January 2010, he was a Senior Antenna Scientist with TNO Defence, Security, and Safety, The Hague, The Netherlands. In February 2010, he became a Full Professor of applied electromagnetism with the EEMCS Department, Technical University of Delft, Delft, The Netherlands, where he formed and leads the THz Sensing Group. His research interests include the analysis and design of antennas with an emphasis on arrays, dielectric lens antennas, wideband antennas, EBG structures, and THz antennas.

Dr. Neto served as an Associate Editor of the IEEE TRANSACTIONS ON ANTENNAS AND PROPAGATION (2008–2013) and IEEE ANTENNAS AND WIRELESS PROPAGATION LETTERS (2005–2013). He is a member of the Technical Board of the European School of Antennas and organizer of the course on antenna imaging techniques. He is a member of the Steering Committee of the Network of Excellence NEWFOCUS, dedicated to focusing techniques in mm and sub-mm wave regimes. In 2011, he was the recipient of the European Research Council Starting Grant to perform research on Advanced Antenna Architectures for THz Sensing Systems. He was the recipient of the H. A. Wheeler Award for the best applications paper of 2008 in the IEEE TRANSACTIONS ON ANTENNAS AND PROPAGATION, the Best Innovative Paper Prize of the 30th ESA Antenna Workshop in 2008, and the Best Antenna Theory Paper Prize of the European Conference on Antennas and Propagation (EuCAP) in 2010. In 2011, he was the recipient of the European Research Council Starting Grant to perform research on advanced antenna architectures for THz sensing systems.